

RESEARCH ARTICLE

On the finite Radon transform for the computational homogenization of conductivity

Lukas Jabs¹  | Matti Schneider^{1,2}

¹Institute of Engineering Mathematics, University of Duisburg-Essen, Essen, Germany

²Department of Flow and Material Simulation, Fraunhofer Institute for Industrial Mathematics ITWM, Kaiserslautern, Germany

Correspondence

Matti Schneider, Institute of Engineering Mathematics, University of Duisburg-Essen, Essen, Germany.
Email: matti.schneider@uni-due.de

Funding information

European Research Council, Grant/Award Number: 101040238; Deutsche Forschungsgemeinschaft, Grant/Award Number: 516929769

Abstract

This paper investigates the computational homogenization of thermal conductivity problems using a finite Radon transform as proposed by Derraz and coworkers, implemented using the Fourier slice theorem to allow utilization of the fast Fourier transform-based frameworks and methods. For the finite Radon transform both the original approach and the consistent approach proposed by Jabs and Schneider are used. The two discretizations are compared to the Moulinec–Suquet discretization using numerical examples. In doing so the convergence of the consistent approach is shown and the discussion of the original Radon approach is extended.

1 | INTRODUCTION

In the field of computational homogenization it is a common occurrence that a material containing only isotropic constituents has anisotropic effective properties, showing the strong influence of the geometry of the microstructure on the effective properties. Accurately predicting and even optimize the behavior of such materials offers a variety of possibilities in the product design. Therefore methods to compute the effective material properties mitigating time consuming and expensive testing are of immediate interest.

To avoid the challenge of creating interface-conforming meshes, the approach of Moulinec–Suquet [1, 2] operates on regular rectangular grids and solves periodic homogenization problems using the computationally highly efficient implementation [3] of the discrete Fourier transform, the fast Fourier transform (FFT). Since the original article a number of novel insights, improvements and extensions have been presented. We refer to the recent review articles [4–6] for an in-depth overview. These findings have proven to be of particular interest in material science to investigate mechanical and thermal conductivity problems.

Using a finite Radon transform instead of the discrete Fourier transform, Derraz et al. [7] proposed a novel approach to thermal homogenization problems. Recently, Jabs and Schneider [8] extended this approach to the homogenization of elasticity problems. A key discovery of the work [8] is the lack of convergence for the original Radon based approach under grid refinement. As a remedy, the consistent finite Radon transform was introduced, which overcomes the aforementioned issues and leads to convergence under grid refinement.

This is an open access article under the terms of the [Creative Commons Attribution](https://creativecommons.org/licenses/by/4.0/) License, which permits use, distribution and reproduction in any medium, provided the original work is properly cited.

© 2024 The Author(s). Proceedings in Applied Mathematics and Mechanics published by Wiley-VCH GmbH.

The article at hand studies thermal homogenization problems. We shed light on whether the techniques developed for elasticity also continue to apply to for thermal conductivity. In Section 2, we give a short summary of the thermal conductivity problem which we address in this paper. In Section 3 we continue this study and give insights into the FFT-based and the Radon based discretizations to solve the thermal conductivity problem. In particular we present the two previously mentioned Radon approaches. The article culminates in Section 4 where we present numerical investigations for Radon based discretizations and compare them to the Moulinec–Suquet discretization. These computational examples reveal that there are significant differences between the two Radon discretizations, but intriguingly we also found cases during our study for which they delivered identical results.

2 | PERIODIC HOMOGENIZATION IN THERMAL CONDUCTIVITY

2.1 | Basic equations

We are interested in the effective thermal conductivity tensor κ^{eff} of a microstructured material given on a periodic rectangular cell $Y = [0, L_1] \times [0, L_2] \times \dots \times [0, L_d]$, where d stands for the spatial dimension and L_i , $i = 1, \dots, d$, refer to the edge lengths of the periodic cell. We suppose that the local conductivity tensor

$$\kappa : Y \rightarrow L(\text{Sym}(d)) \quad (1)$$

is given on the cell Y . Here, $L(A)$ denotes the set of linear mappings on the vector space A and $\text{Sym}(d)$ refers to the (vector) space of symmetric $d \times d$ tensors. With the constitutive data (1) at hand, the underlying equations for the thermal conductivity problem [9] read

$$\mathbf{q}(\mathbf{x}) = \kappa(\mathbf{x})[\zeta(\mathbf{x})], \quad \text{div}(\mathbf{q}(\mathbf{x})) = 0 \quad \text{and} \quad \zeta(\mathbf{x}) = \bar{\zeta} - \nabla\theta(\mathbf{x}), \quad (2)$$

where $\nabla\theta$ denotes the gradient of the temperature fluctuation, \mathbf{q} refers to the heat flux, $\bar{\zeta} = \langle \zeta \rangle_Y$ stands for the macroscopic temperature gradient and $\langle \cdot \rangle_Y = \frac{1}{|Y|} \int_Y \cdot dx$ is a short-hand notation for the volume average of a field variable over the cell Y . The constitutive law $\mathbf{q}(\mathbf{x}) = \kappa(\mathbf{x})[\zeta(\mathbf{x})]$ is known as Fourier's law. The effective heat flux arises as the volume average of the local heat flux $\mathbf{q}(\mathbf{x})$ and is given by

$$\mathbf{q}^{\text{eff}}(\bar{\zeta}) = \langle \kappa[\zeta] \rangle_Y. \quad (3)$$

Due to the linearity of the Equations (2), the effective constitutive law is of Fourier type with the effective conductivity tensor defined via $\kappa^{\text{eff}} \left[\bar{\zeta} \right] = \langle \kappa[\zeta] \rangle_Y$.

2.2 | Lippmann–Schwinger reformulation

Introducing a homogeneous reference conductivity $\kappa^0 = \kappa^0 \mathbf{Id}$, the problem given in Equation (2) may be equivalently reformulated in terms of the Lippmann–Schwinger equation [10–12]

$$\zeta = \bar{\zeta} - \mathbf{\Gamma}^0[\tau], \quad \text{with the heat-flux polarization} \quad \tau = (\kappa - \kappa^0)[\zeta] \quad (4)$$

and the Eshelby–Green operator $\mathbf{\Gamma}^0 = \frac{1}{\kappa^0} \nabla(\text{div}\nabla)^\dagger \text{div}$, where $(\cdot)^\dagger$ refers to the Moore–Penrose pseudoinverse. The suggestive fixed-point form of Equation (4) gives rise to an iterative scheme, which is also known as the basic scheme [1, 2]

$$\zeta^{k+1} = \bar{\zeta} - \mathbf{\Gamma}^0[\tau^k] \quad \text{with} \quad \tau^k = (\kappa - \kappa^0)[\zeta^k]. \quad (5)$$

3 | REFORMULATIONS AND DISCRETIZATIONS

3.1 | The classical Fourier approach

Fourier series allow us to express a square-integrable function $f \in L^2(Y)$ in terms of an expansion of the form

$$f(\mathbf{x}) = \sum_{\tilde{\xi} \in \mathbb{Z}^d} \hat{f}(\tilde{\xi}) \exp(i\mathbf{x} \cdot \tilde{\xi}), \quad \tilde{\xi}_k = \frac{2\pi}{L_k} \xi_k, \quad k = 1, 2, \dots, d, \quad (6)$$

where the Fourier coefficients $\hat{f}(\tilde{\xi})$ are given by weighted volume averages in the following manner

$$\hat{f}(\tilde{\xi}) = \frac{1}{|Y|} \int_Y f(\mathbf{x}) \exp(-i\mathbf{x} \cdot \tilde{\xi}) dx, \quad \tilde{\xi} \in \mathbb{Z}^d. \quad (7)$$

Using the differentiation properties of the Fourier series allows us to express the action of the Eshelby–Green operator appearing in the Lippmann–Schwinger equation (Equation 4) in the form

$$\left(\Gamma^0[\tau]\right)(\mathbf{x}) = \sum_{\tilde{\xi} \in \mathbb{Z}^d} \hat{\Gamma}^0(\tilde{\xi}) [\hat{\tau}(\tilde{\xi})] \exp(i\mathbf{x} \cdot \tilde{\xi}) \quad (8)$$

with explicit representation of the Fourier coefficients $\hat{\Gamma}^0[\hat{\tau}(\tilde{\xi})]$ given by

$$\Gamma^0(\tilde{\xi}) = \frac{1}{\kappa^0 \tilde{\xi} \cdot \tilde{\xi}} \tilde{\xi} \otimes \tilde{\xi}, \quad \tilde{\xi} \neq \mathbf{0} \quad \text{and} \quad \Gamma^0(\mathbf{0}) = \mathbf{0}. \quad (9)$$

For details on the convergence behavior, the error estimates and various solving schemes for the iterative scheme of the Lippmann–Schwinger equation (Equation 5), we refer to the review articles [4–6]. These works also offer guidance on various discretization schemes, in particular the Moulinec–Suquet discretization [1, 2]. For the latter the Fourier series is truncated to trigonometric polynomials. The Moulinec–Suquet discretization is based on trigonometric polynomials and an associated trigonometric interpolation rule, see the articles [1, 2] for details.

3.2 | The alternative Radon approach

An alternative representation of a square integrable function $f \in L^2(Y)$ is given by the Radon series [13]. More precisely, such a function may be expressed in the form

$$f(\mathbf{x}) = \langle f \rangle_Y + \sum_{\tilde{\xi} \in \mathcal{G}^d} \left(\check{f}_{\tilde{\xi}}(\mathbf{x} \cdot \tilde{\xi}) - \langle f \rangle_Y \right). \quad (10)$$

There are different ways to represent the term $\check{f}_{\tilde{\xi}}(\mathbf{x} \cdot \tilde{\xi})$, see Jabs and Schneider [8]. One of them is given by

$$\check{f}_{\tilde{\xi}}(s) = \sum_{k \in \mathbb{Z}} \hat{f}(k \tilde{\xi}) \exp(iks), \quad s \in [0, 2\pi]. \quad (11)$$

In Equation (10) the vectors $\tilde{\xi} \in \mathbb{Z}^d$ refer to generators of cyclic groups $k\tilde{\xi} \subseteq \mathbb{Z}^d$. To specify the set of generators \mathcal{G}^d , two conditions are sufficient:

1. The greatest common divisor of all components of the generator is 1.
2. The first non-zero component is positive.

The first condition assures that the cyclic groups do not intersect outside of the zero frequency. The second condition avoids ambiguity in the definition, since the vectors $-\xi$ and ξ create the same cyclic group and fulfill the first condition [8]. The form presented in Equation (11) offers a close link of the Radon series to the Fourier series, in the sense that it allows us to represent the Radon transform of a d-dimensional function as a sum of one dimensional Fourier series. Interestingly, the Radon series (Equation 10) is entirely based on real-valued functions – in contrast to the Fourier series which critically relies on complex numbers.

In the discrete case, the representation of the function f on the discrete cell $Y_N \equiv \mathbb{Z}_N^d \equiv (\mathbb{Z}/(N\mathbb{Z}))^d$ is presented as

$$f(\mathbf{I}) = f_0 + \sum_{\xi \in \mathcal{G}_N^d} (\check{f}(\mathbf{I} \cdot \xi) - f_0) \text{ with } \mathbf{I} \in Y_N, \quad (12)$$

where f_0 refers to the average of the function f over the cell Y_N [8]. The set of generators \mathcal{G}_N^d , as well as the cyclic groups

$$C(\xi) = \{k\xi \pmod N \mid k \in \mathbb{Z}\} \quad (13)$$

are finite. As for the continuous case the set of generators has to contain all generators necessary to create a family of cyclic groups, which do not intersect except for the zero vector but create a covering of the discrete cell Y_N . This requirement does not lead to a unique set of generators, but requires the grid lattice to have an equal prime number of grid points in each spatial direction. The classical set of generators, for three dimensional problems, fulfilling these requirements [14] is given as follows

$$\mathcal{G}_N^d = \{(1, 0, 0)\} \cup \{(a, 1, 0) \mid a \in \mathbb{Z}_N\} \cup \{(a, b, 1) \mid a, b \in \mathbb{Z}_N\}. \quad (14)$$

If this set of generators is used for the Radon transform, we refer to the corresponding discretization as the finite Radon discretization (FRD).

For mechanical problems, this choice of generators was shown to lead to certain disadvantages w.r.t. the frequencies utilized in the calculation of the Gamma operator (Equation 9) [8]. For example, this selection of generators results in a representation of the homogenization problem that does not converge to the continuous solution under grid refinement. There are also certain frequencies which are neglected regardless of the resolution.

A proposed remedy [8] for this problem is to select the elements of the set of generators as

$$\xi_C = \operatorname{argmin}\{\|\xi\|_\infty \mid \xi \in \mathbb{Z}^d \setminus \{0\} \text{ and } \xi > -\xi, \text{ s.t. } \xi \in C \pmod N\}, \quad (15)$$

where C denotes a cyclic group w.r.t. the modular arithmetic, as seen in Equation (13). The condition $\xi > -\xi$ stands for a lexicographic ordering, assuring that the first non-zero component is positive. If such a set of generators is used, we refer to the corresponding discretization as the consistent Radon discretization (CRD).

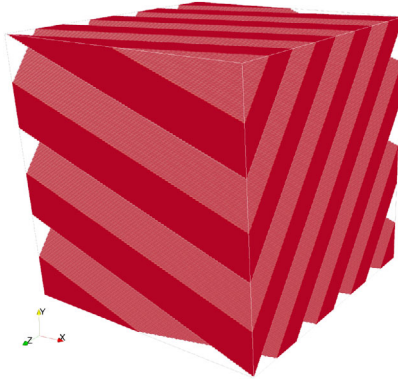
Both choices of generators lead to a discrete Lippmann–Schwinger equation for thermal conductivity in the form of

$$\begin{aligned} \zeta(\mathbf{I}) &= \bar{\zeta} - \sum_{\xi \in \mathcal{G}_N^d} (\check{\zeta}_\xi(\mathbf{I} \cdot \xi) - \bar{\zeta}) \\ &= \bar{\zeta} - \sum_{\xi \in \mathcal{G}_N^d} \left(\sum_{k \in \mathbb{Z}_N} [\hat{\Gamma}^0(\xi) \hat{t}(k\xi) \exp(k\xi \cdot \mathbf{I})] - \bar{\zeta} \right), \end{aligned} \quad (16)$$

where the 0-homogeneity of the Eshelby–Green operator is used, i.e., $\Gamma^0(k\xi) = \Gamma^0(\xi)$ holds for all $k \in \mathbb{Z} \setminus \{0\}$. It is advisable to use the Fourier slice theorem (Equation 11) to compute the iterative scheme associated to the Lippmann–Schwinger Equation (16) via the discrete Fourier transform [8], s.t. fast and existing implementations can be used.

TABLE 1 Material parameters for the simulations.

Isotropic	$\kappa = 1 \frac{W}{m \cdot K}$		
Isotropic conductive	$\kappa = 100 \frac{W}{m \cdot K}$		
Orthotropic	$\kappa_1 = 1 \frac{W}{m \cdot K}$	$\kappa_2 = 10 \frac{W}{m \cdot K}$	$\kappa_3 = 100 \frac{W}{m \cdot K}$

**FIGURE 1** Microstructure of a tilted laminate with normal orientation $\mathbf{n} = (1, 3, 4)^\top$ and a resolution of 256^3 voxels.

4 | NUMERICAL INVESTIGATIONS

4.1 | Setup

The computations for this paper were run on a system with an Intel® Core™ i7-1360P and 32GB of RAM. The code for the homogenization was implemented in Python using Cython extensions. The parallelization was implemented using OpenMP. The linear system was solved with the conjugate gradient method [15–17]. The convergence was assessed, up to a tolerance of 10^{-5} , according to the criterion [6, eq. 3.41]. The material parameters for the subsequent simulations are given in Table 1.

4.2 | Tilted laminates

The exact representation of certain tilted laminates is an outstanding feature of the Radon discretizations [7, 8]. We want to check whether this property also holds true for the CRD (15) in the case of thermal conductivity problems and if we can reproduce and extend on some of the findings of Derraz et al. [7]. Furthermore, the known analytical solution for the laminate makes it a predestined microstructure to start the investigations into the behavior of discretizations. In Figure 1, the microstructure of interest for the following calculations is shown. More precisely, we present a voxelized volume cell for a laminate structure with a normal orientation of $\mathbf{n} = (1, 3, 4)^\top$. The microstructure is comprised of two phases, a highly conductive isotropic phase and another isotropic phase, whose conductivity was normalized to unity. Table 1 lists the material parameters for the constituent phases.

If the local heat flux fields are examined for a prescribed temperature gradient of $\bar{\zeta} = 1\mathbf{e}_y$, results similar to those of the elastic laminated materials [8] are found. The local heat flux field of the Moulinec–Suquet discretization (Figure 2A) shows close resemblance to the analytical solution, which is constant in each phase. However, there are strong ringing artifacts in the lamination direction at the phase boundary. For the local heat flux field of the FRD discretization (Figure 2B), on the other hand, the local field represents the analytical solution exactly. More precisely, there are no artifacts or other disturbances and individual phases show the expected constant heat flux fields. In the case of the CRD, the heat flux field (Figure 2C) is identical to the one of the FRD, that is, it also represents the analytical solution exactly.

Looking at the relative error between the analytical solution for the effective conductivity and the computationally determined effective conductivity, it is no surprise that the exact representation of the local fields also leads to an exact representation of the effective values as can be seen in Figure 3. Here the FRD and the CRD both have an exact

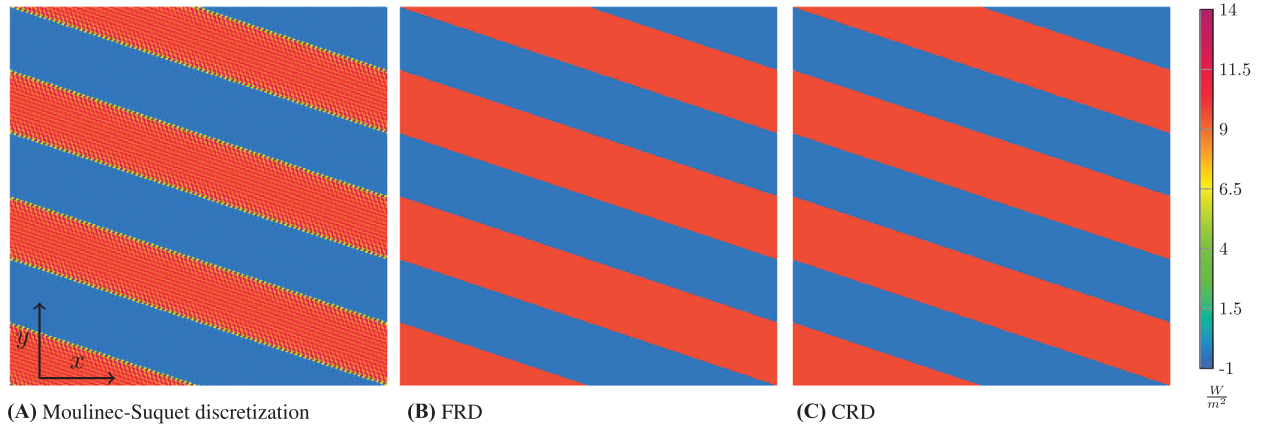


FIGURE 2 Local heat flux for a prescribed temperature gradient of $\bar{\zeta} = 1 \frac{W}{m} \mathbf{e}_y$ and different discretizations in the direction \mathbf{e}_x .

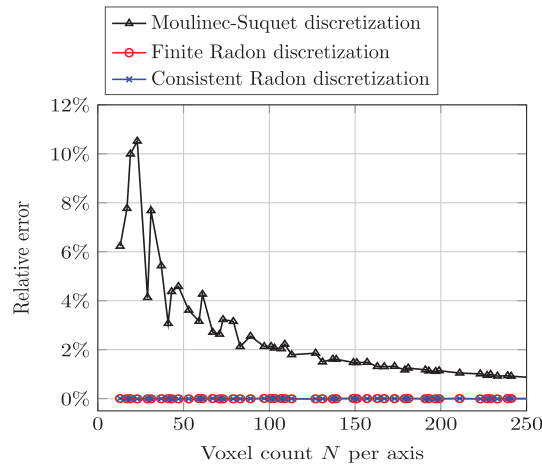


FIGURE 3 Relative error for the discretizations compared to the analytical solution for increasing resolutions.

representation of the analytical solution up to the required precision determined by the solver. For the Moulinec–Suquet discretization, the convergence under grid refinement is visible, so that for voxel counts close to 250^3 , the relative error has decreased to approximately 1%.

To investigate the influence of an increasing material contrast $\mu \in \mathbb{R}_{\geq 1}$, the conductivity of the first phase is fixed to $\kappa_1 = 1 \frac{W}{m \cdot K} \mathbf{Id}$, while scaling the conductivity of the second phase $\kappa_2 = \mu \frac{W}{m \cdot K} \mathbf{Id}$. The findings presented in Figure 4 show an increasing error for the Moulinec–Suquet discretization for the increasing material contrast, while the FRD and the CRD possess exact solutions up to the computational precision.

4.3 | A Spherical inclusion

Jabs and Schneider [8] showed that the FRD discretization does not converge under grid refinement for the elasticity problem. Derraz et al. [7], on the other hand, report that the solution for the effective conductivity using the FRD is in close enough proximity to the Moulinec–Suquet discretization to assume convergence. To analyze the behavior of the FRD more closely, we compare the results of the FRD with those of the CRD and the Moulinec–Suquet discretization for a single spherical inclusion. The Moulinec–Suquet discretization is chosen as a reference as its convergence behavior is proven [18–20]. Each cell contains one spherical inclusion with a diameter of $9/10$ of the edge length, resulting in a inclusion volume fraction of approximately 38.17%, see Figure 5. We furnish the surrounding matrix material with the isotropic material, whereas the orthotropic material is assigned to the spherical inclusions, see Tab. 1. With this setup at hand, we investigate the behavior of the discretizations under grid refinement. In Figure 6, the 22- and the 33- component

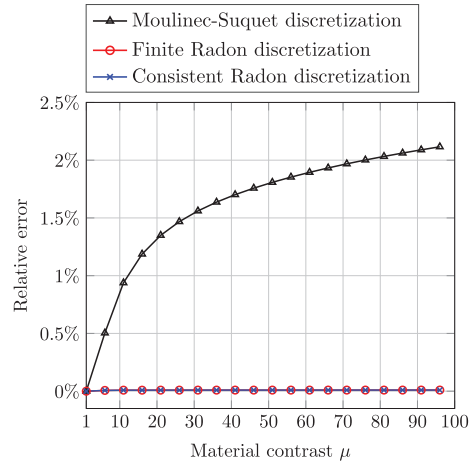


FIGURE 4 Influence of the material contrast on the precision of the discretizations.

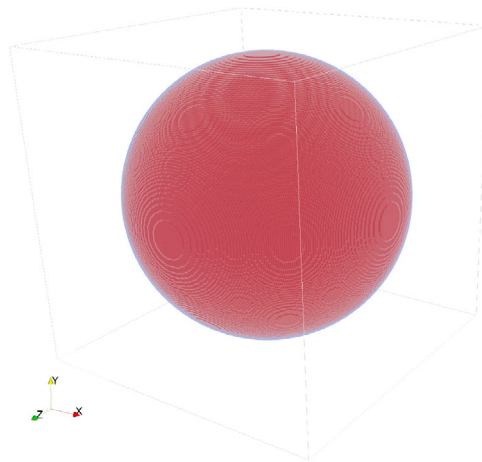


FIGURE 5 Microstructure of the spherical inclusion, with 251^3 voxels.

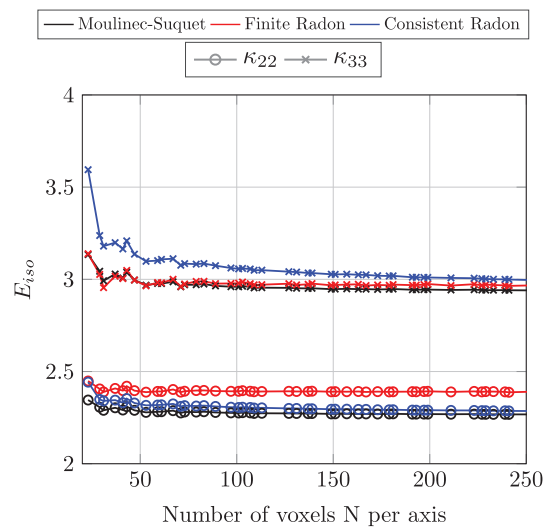


FIGURE 6 Components of the effective conductivity tensor under grid refinement.

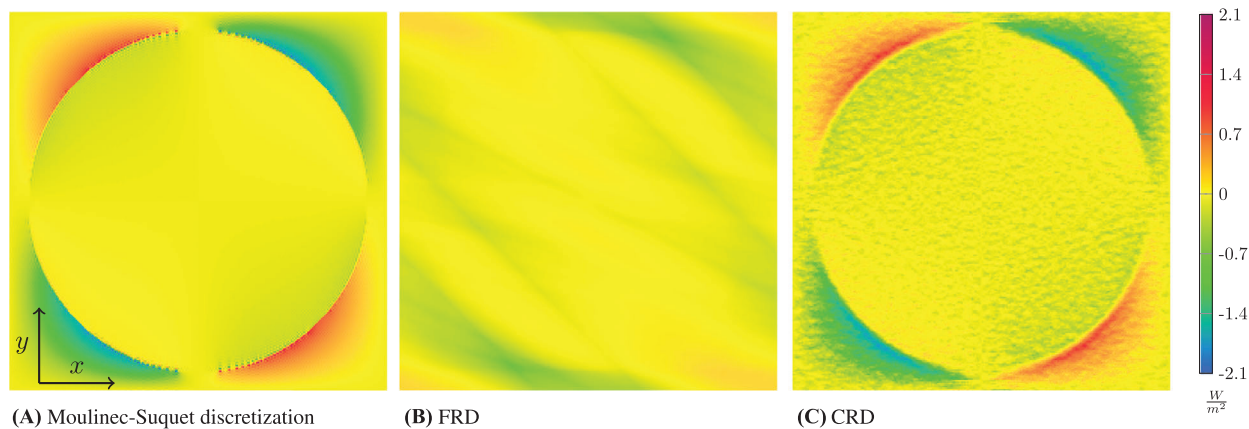


FIGURE 7 Local heat flux for a prescribed temperature gradient of $\bar{\zeta} = 1 \frac{W}{m} \mathbf{e}_y$ and different discretizations in the direction \mathbf{e}_x .

of the effective conductivity tensor κ^{eff} are shown. Two things should be highlighted. For a start the effective conductivities calculated utilizing the FRD are, as Derraz et al. [7] already have shown, very close to the solution presented by the Moulinec–Suquet discretization. For κ_{33}^{eff} , the effective conductivity resulting from the Moulinec–Suquet discretization is in fact more closely aligned with the result determined by employing the FRD than it is with the result determined using the CRD. However, for κ_{22}^{eff} , the effective conductivity identified using the FRD does not converge to the value resulting from the Moulinec–Suquet discretization. In contrast, the effective conductivity brought about by the CRD in both cases slowly converges to the value identified using the Moulinec–Suquet discretization, which is in accordance with the findings of Jabs and Schneider [8].

These findings are emphasized by Figure 7A–C. In this figure, the heat flux in x -direction is shown for all three considered discretizations. As in the case for the elasticity problem [8], the Moulinec–Suquet discretization gives rise to a smooth solution field apart from the ringing artifacts. The CRD shows strong artifacts, which may be interpreted as “noise”, while still showing the same features as the Moulinec–Suquet discretization. Meanwhile, the solution field of the FRD differs drastically: The sphere is no longer recognizable and the symmetry of the microstructure is not represented.

5 | CONCLUSION

We aimed at extending the understanding of the finite Radon transform in the context of computational homogenization problems, with a focus on thermal conductivity. Therefore, the thermal conductivity problem was reintroduced and an outline of the FFT-based homogenization for thermal conductivity problems was presented, where the work of Derraz et al. [7] and Jabs and Schneider [8] represent closely related contributions. Subsequently, we briefly discussed the two Radon-based discretization schemes, where the CRD was motivated as a possible remedy to the shortcomings of the FRD. Finally, numerical investigations were given and discussed. In particular, the aforementioned shortcomings of the FRD were of interest. First a laminate microstructure was investigated and we were able to show that the CRD does represent them exactly. A fact that was already known for the FRD [7]. Secondly a spherical inclusion was investigated, and we showed that the shortcomings found previously for elasticity are also present for thermal conductivity problems. However, their extent appears to be less significant than in the elastic case. Nevertheless the deviation is systematic and based on the fact that certain frequencies are neglected when using the FRD.

The presented findings allow us to conclude that, in general, the FRD is in fact also not convergent under grid refinement for the case of thermal conductivity and that the CRD fixes the shortcomings of the FRD, as it converges under grid refinement.

ACKNOWLEDGMENTS

The support of the European Research Council through the Horizon Europe program (Project No. 101040238) is gratefully acknowledged by M.S. L.J. acknowledges the funding by the Deutsche Forschungsgemeinschaft (DFG, German Research Foundation, Grant No. 516929769). We thank the anonymous reviewer for the constructive criticism and the interest in our work.

Open access funding enabled and organized by Projekt DEAL.

DATA AVAILABILITY STATEMENT

The data that support the findings of this study are available from the corresponding author upon reasonable request.

ORCID

Lukas Jabs  <https://orcid.org/0000-0002-8733-5908>

REFERENCES

1. Moulinec, H., & Suquet, P. (1994). A fast numerical method for computing the linear and nonlinear mechanical properties of composites. *Comptes Rendus de l'Académie des Sciences. Série II*, 318, 1417–1423.
2. Moulinec, H., & Suquet, P. (1998). A numerical method for computing the overall response of nonlinear composites with complex microstructure. *Computer Methods in Applied Mechanics and Engineering*, 157, 69–94.
3. Frigo, M., & Johnson, S. G. (2005). The Design and Implementation of FFTW3. *Proceedings of the IEEE*, 93, 216–231.
4. Lebensohn, R. A., & Rollett, A. D. (2020). Spectral methods for full-field micromechanical modelling of polycrystalline materials. *Computational Materials Science*, 173, 109336.
5. Segurado, J., Lebensohn, R. A., & LLorca, J. (2018). Chapter One – Computational Homogenization of Polycrystals. *Advances in Applied Mechanics*, 51, 1–114.
6. Schneider, M. (2021). A review of nonlinear FFT-based computational homogenization methods. *Acta Mechanica*, 232, 2051–2100.
7. Derraz, M. R., Boukour, M., El Mamouni, A., & El Omri, A. (2022). Three-dimensional finite radon transform and linear homogenization. *Advanced Intelligent Systems for Sustainable Development (AI2SD'2020)* (Vol. 1418, pp. 164–182). Springer International Publishing.
8. Jabs, L., & Schneider, M. (2024). A consistent discretization via the finite radon transform for FFT-based computational micromechanics. *Computational Mechanics*, 1–20. <https://doi.org/10.1007/s00466-024-02542-9>
9. Dorn, C., & Schneider, M. (2019). Lippmann-Schwinger solvers for the explicit jump discretization for thermal computational homogenization problems. *International Journal for Numerical Methods in Engineering*, 118, 631–653.
10. Zeller, R., & Dederichs, P. H. (1973). Elastic Constants of Polycrystals. *physica status solidi*, 55, 831–842.
11. Kröner, E. (1977). Bounds for effective elastic moduli of disordered materials. *Journal of the Mechanics and Physics of Solids*, 25, 137–155.
12. Mura, T. (1987). *Micromechanics of defects in solids*. Martinus Nijhoff Publishers.
13. Gelfand, I. M., Gindikin, S. G., & Graev, M. I. (2003). Selected topics in integral geometry. *Translations of mathematical monographs* (Vol. 220). AMS.
14. Boukour, M., & El Omri, A. (2019). A 3D finite radon transform. *Journal of Mathematics and System Science*, 9, 64–69.
15. Zeman, J., Vondřejc, J., Novák, J., & Marek, I. (2010). Accelerating a FFT-based solver for numerical homogenization of periodic media by conjugate gradients. *Journal of Computational Physics*, 229, 8065–8071.
16. Brisard, S., & Dormieux, L. (2010). FFT-based methods for the mechanics of composites: A general variational framework. *Computational Materials Science*, 49, 663–671.
17. Schneider, M. (2020). A dynamical view of nonlinear conjugate gradient methods with applications to FFT-based computational micromechanics. *Computational Mechanics*, 66, 239–257.
18. Brisard, S., & Dormieux, L. (2012). Combining Galerkin approximation techniques with the principle of Hashin and Shtrikman to derive a new FFT-based numerical method for the homogenization of composites. *Computer Methods in Applied Mechanics and Engineering*, 217, 197–212.
19. Vondřejc, J., Zeman, J., & Marek, I. (2014). An FFT-based Galerkin method for homogenization of periodic media. *Computers & Mathematics with Applications*, 68, 156–173.
20. Schneider, M. (2015). Convergence of FFT-based homogenization for strongly heterogeneous media. *Mathematical Methods in the Applied Sciences*, 38, 2761–2778.

How to cite this article: Jabs, L., & Schneider, M. (2024). On the finite Radon transform for the computational homogenization of conductivity. *Proceedings in Applied Mathematics and Mechanics*, 24, e202400189. <https://doi.org/10.1002/pamm.202400189>

DuEPublico

Duisburg-Essen Publications online

UNIVERSITÄT
DUISBURG
ESSEN

Offen im Denken

ub | universitäts
bibliothek

This text is made available via DuEPublico, the institutional repository of the University of Duisburg-Essen. This version may eventually differ from another version distributed by a commercial publisher.

DOI: 10.1002/pamm.202400189

URN: urn:nbn:de:hbz:465-20250224-144639-1



This work may be used under a Creative Commons Attribution 4.0 License (CC BY 4.0).